nature materials

LETTERS

PUBLISHED ONLINE: 27 JULY 2014 | DOI: 10.1038/NMAT4037

Surface-initiated self-healing of polymers in aqueous media

B. Kollbe Ahn[1†], Dong Woog Lee[2†], Jacob N. Israelachvili[2*] and J. Herbert Waite[3*]

Polymeric materials that intrinsically heal at damage sites under wet or moist conditions are urgently needed for biomedical and environmental applications[1–6]. Although hydrogels with self-mending properties have been engineered by means of mussel-inspired metal-chelating catechol-functionalized polymer networks[7–10], biological self-healing in wet conditions, as occurs in self-assembled holdfast proteins in mussels and other marine organisms[11,12], is generally thought to involve more than reversible metal chelates. Here we demonstrate self-mending in metal-free water of synthetic polyacrylate and polymethacrylate materials that are surface-functionalized with mussel-inspired catechols. Wet self-mending of scission in these polymers is initiated and accelerated by hydrogen bonding between interfacial catechol moieties, and consolidated by the recruitment of other non-covalent interactions contributed by subsurface moieties. The repaired and pristine samples show similar mechanical properties, suggesting that the triggering of complete self-healing is enabled underwater by the formation of extensive catechol-mediated interfacial hydrogen bonds.

All polymeric materials suffer damage in the course of their functional lifetimes. Few, if any, completely heal at damage sites. Despite recent progress in the design of self-mending polymeric materials based on crack-activated crosslinking[1], light[2], heat[3] or other external stimuli[4], these remain less than perfectly healed, and, in the case of polymers in wet environments, self-healing technologies are even more limited than those engineered for dry conditions. Mussel adhesive holdfasts exhibit significant self-healing capabilities[11,12], although the molecular mechanisms involved are poorly understood. Notwithstanding this, the self-mending adhesion and cohesion of isolated dopa (3,4-dihydroxyphenyl-L-alanine)-containing adhesive proteins were shown to rely critically on maintaining dopa in an acidic and reducing environment[13,14]. Significantly different conditions are required to recapitulate the self-healing cohesion of tris-dopa-Fe^{3+}-mediated complexes in proteins and polymers[7–9,15]. Such results increasingly suggest the importance of dopa, but also its subtle and diverse interfacial reactivity vis-à-vis the traditional and still widely held view that dopa, and catechols generally, function primarily as crosslinkers after their 2-electron oxidation to quinones[16]. To better assess the contribution of catechol to polymer self-healing in a reducing (pH 3), metal-free wet environment, we prepared a material from common, water-insoluble synthetic acrylic polymers having a catechol-functionalized surface. These materials are completely self-healing in a process initiated by catechol-mediated interfacial hydrogen bonding, and consolidated by follow-up interactions (for example, hydrophobic and steric) after a brief compression ($\sim 6 \times 10^4$ Pa). The crucial and robust roles played by catecholic hydrogen bonding in re-establishing contact between the fragments, then giving way to other interactions, were completely unexpected and may inspire the wet repair of other polymers and tissues.

Surface rearrangement plays a critical role in polymeric interface properties[17]; therefore, two polymers with different moduli were prepared to study the surface changes initiated during self-healing. Semi-rigid (Young's modulus, $E \sim 1.3$ MPa) and rigid polymer rods ($E \sim 350$ MPa) were cast from triethylsilane-blocked catecholacrylate and catecholmethacrylate monomers, respectively, by free radical ultraviolet polymerization (Supplementary Fig. 1). The rods were bisected using a new scalpel blade; the two pieces were soaked in a series of dilute buffers with increasing pH (range: 3–10), respectively, for 20 min. Subsequently, the cut ends were rejoined under light compression ($\sim 6 \times 10^4$ Pa) for 2 min in water (pH 3, 7 or 10). pH 3 activates the catechol functionalities on the surfaces by removing the triethylsilyl-protecting groups[14] (Fig. 1), whereas triethylsilyl catechols at pH 7 and 10 remain blocked (protected). Catechols internalized in the bulk remained blocked at all conditions (pH 3, 7 and 10). To avoid catechol oxidation and related ring coupling, experiments involving exposed surface catechols were performed at pH 3, where the high quinone reduction potential ($E_0 \sim 0.38$ V; ref. 18) assures catechol stability[19]. Semi-rigid rods with exposed surface catechols never failed near the contact region, whereas rigid rods sometimes ruptured in the contact region (Fig. 1a,b). In the latter case, when breakage occurred in the contact region, the two pieces were repeatedly brought into contact and pulled in tension until a non-contact breakage occurred. During cyclic testing, the healed (the contact region) and undamaged portions of the rigid polymer rods exhibited similar mechanical properties (Fig. 1c). When surface treatments and experiments were carried out at pH 7 and 10, catechols remain blocked by silyl protection. Under these conditions, the semi-rigid polymer rods with blocked surface catechols always failed in the contact area, whereas the rigid polymer rods with blocked surface catechols showed no bonding whatever (Fig. 1c). These results highlight the importance of catechols at the self-healing interface, and suggest that only reversible interactions (for example, hydrogen bonds) take place during the initial stages of self-healing. Details of this surface-mediated healing system are discussed in depth later.

The Bell theory predicts that a bidentate hydrogen bond, such as that between a catechol donor and a surface acceptor, has a binding lifetime that is 10^6 times longer than the monodentate hydrogen-bond[20]; experiment confirms that the catechol-mediated bidentate hydrogen bond is stronger than the monodentate hydrogen bond (that is, $E_{\text{bidentate}} \sim 2E_{\text{monodentate}}$, or $\tau_{\text{bidentate}} \sim 10^6 \tau_{\text{monodentate}}$) (refs 13,20). In addition, previous studies of the intermolecular hydrogen bonds between phenolic hydroxyls[21], catechol and

[1]Marine Science Institute, University of California, Santa Barbara, California 93106, USA, [2]Chemical Engineering, University of California, Santa Barbara, California 93106, USA, [3]Molecular, Cellular and Developmental Biology, University of California, Santa Barbara, California 93106, USA. †These authors contributed equally to this work. *e-mail: jacob@engineering.ucsb.edu; waite@lifesci.ucsb.edu

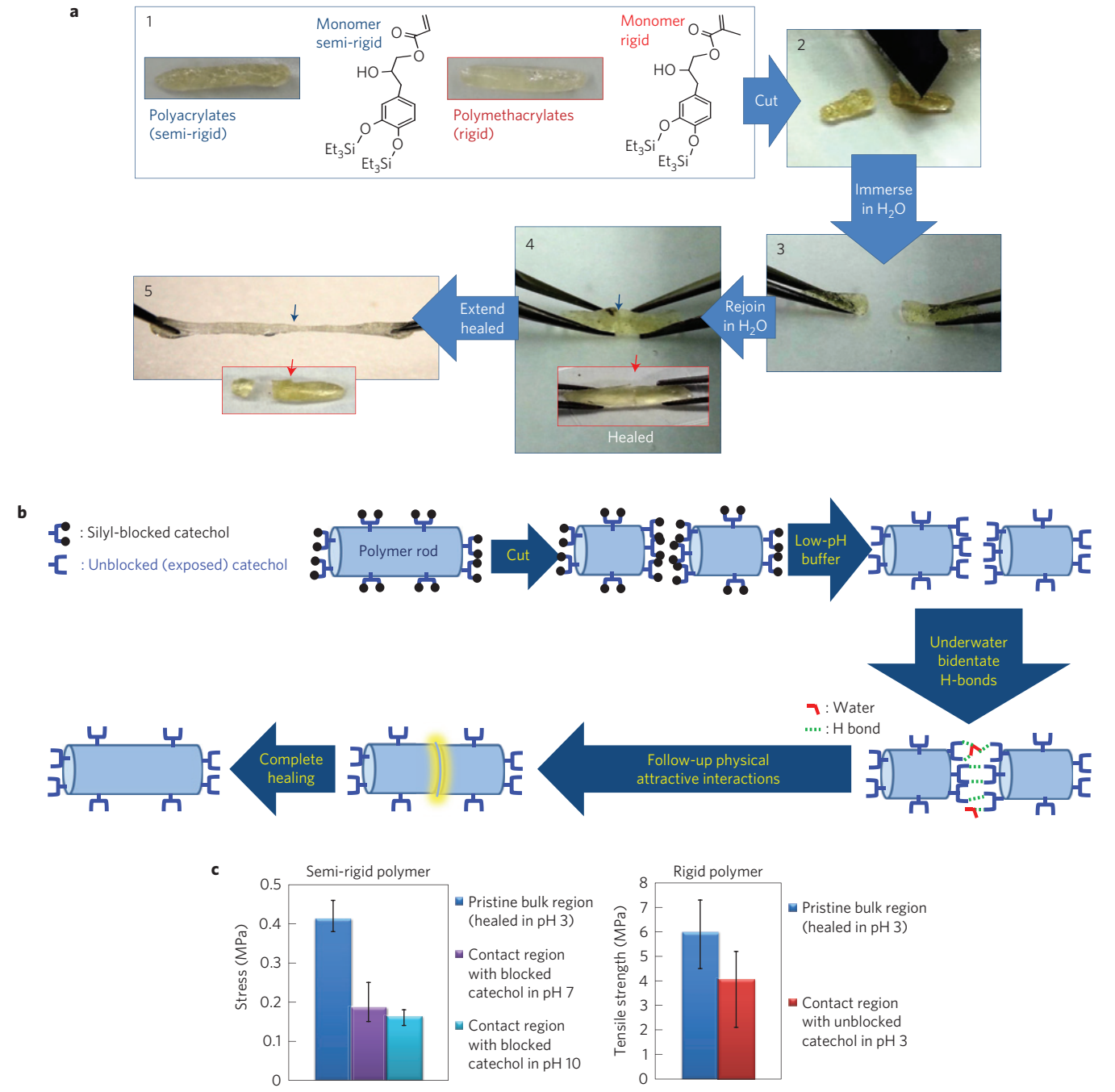

Figure 1 | Schematic diagram of the steps entailed in polymer-rod healing studies. a, Polymer rods (1; semi-rigid, blue rectangle; rigid, red rectangle) were processed as follows: bisected (2), immersed in H_2O (pH 3 buffer) at room temperature (3), brought into contact (4) and pulled in tension (5). The blue (semi-rigid) and red (rigid) arrows denote the location of the healed incisions. **b**, Self-healing scheme. **c**, Average tensile strength of the samples (error bars indicate standard deviation, $n=3$).

quinone[22] in storage devices (ferroelectrics), two neighbouring catechols (hydrogen-bond length 2.12 Å, ~3.0 kJ mol^{-1}; ref. 23), and multivalent intermolecular hydrogen bonds of catechols in water[24], concur that closely stacked catechols at surfaces provide strong intermolecular hydrogen bonds when brought into contact.

The synchrotron near-edge X-ray absorption fine structure (NEXAFS; Fig. 2) of the polymers confirms that catechol moieties exist only at the polymer/water interface, whereas catechols buried in the bulk remain silyl-blocked. It is noteworthy that of the analytical methods used, including synchrotron grazing incidence wide-angle X-ray scattering (Supplementary Fig. 3), X-ray reflectivity (Supplementary Fig. 4), and confocal Raman microscopy (Supplementary Fig. 5), only synchrotron NEXAFS (highly surface sensitive) detected small surface-associated intensity changes (Fig. 2). The others were unable to differentiate the interface from the bulk. In NEXAFS, a plot of the π^* intensity in polymers with exposed catechols increases slightly with an increasing incident angle (Fig. 2b), indicating a slightly ordered orientation of aromatic rings on the surface, whereas in polymers with blocked catechols random distribution is evident[25,26] (Fig. 2c). In addition, the π^* orbital signal is more pronounced for polymers with exposed catechols compared with the blocked controls (Fig. 2d), suggesting that removal of the silyl groups may enable more catechols to populate the interface. Given the low uncertainty of the NEXAFS measurements, the

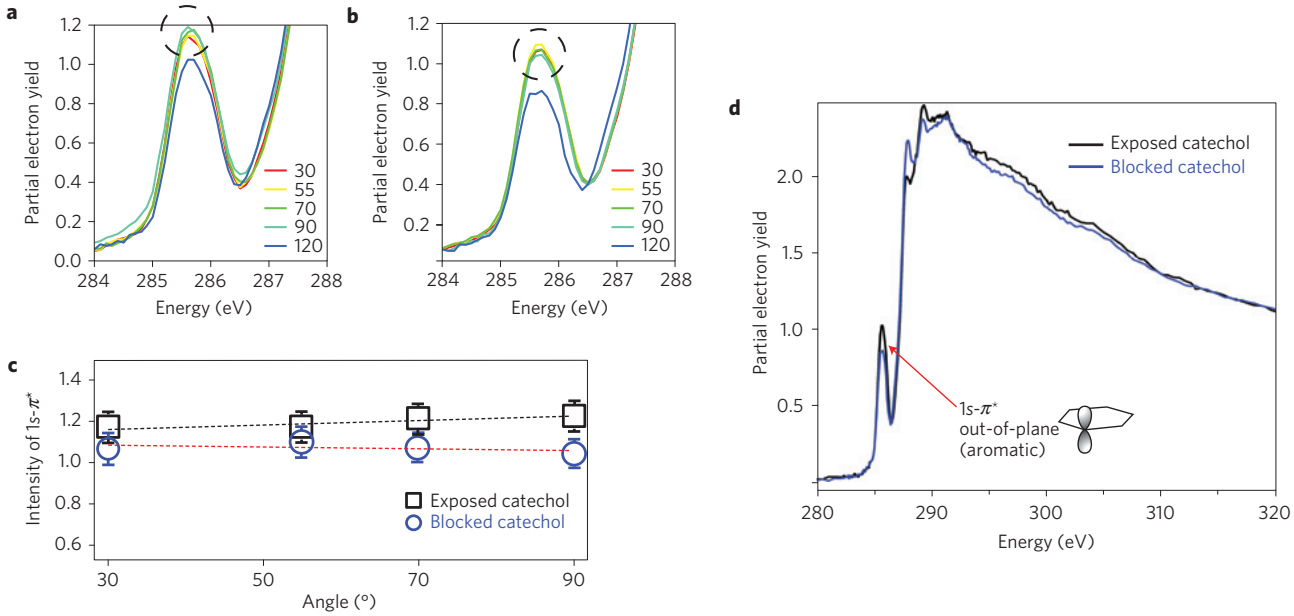

Figure 2 | NEXAFS spectra of catechol-functionalized polymer samples at incident radiation angles ranging from 30° to 120°. a,**b**, Partial electron yields for exposed (**a**) and blocked (**b**) catecholic polymer. The dashed circles indicate the peaks whose intensities are plotted in **c**. **c**, π^* orbitals plot. Error bars indicate the maximum uncertainty (~2%) of the electron yield. **d**, Incident radiation angle at 120°.

differences are likely to be significant[25,26]. Consistent with NEXAFS, X-ray photoelectron spectroscopy showed ~10% decrease in the Si 2*p* signal following acid treatment (Supplementary Fig. 6).

Contact-angle measurements of water droplets on all prepared polymer surfaces indicate a decreasing hydrophobicity with time, suggesting that the polymeric surfaces are undergoing a reversible rearrangement[17] (Supplementary Fig. 7). These surface-group 'turnover' effects are known to change the interfacial adhesion energy and, therefore, the contact angle. Increasing adhesion with contact time, t_c, has been seen in many systems[27]. These phenomena directly depend on bulk and (especially surface) molecular mobility, stiffness, and viscosity of the material, and determine the time frame in which an increase in adhesion starts and plateaus.

To elucidate the interfacial mechanism of adhesion related to self-healing, a surface forces apparatus (SFA) was used to investigate the contact time (t_c)-dependent adhesion at the interface of the self-healing (contact) area (Fig. 3a,b).

Adhesion forces (F_{ad}) between symmetric surfaces were measured as a function of t_c (Fig. 3) at a fixed load (L) of 250 mN. For soft polymers (synthesized as the semi-rigid polymer but with lower polymerization; see Supplementary Methods), F_{ad} of the exposed and blocked catecholic polymers increased monotonically with time from 700 to 1,500 mN and from 100 to 1,210 mN, respectively, with t_c increasing from 5 to 120 s (Fig. 3c). After a contact time of $t_c \sim 120$ s, the F_{ad} between two exposed catecholic polymer surfaces (film thickness ~25 μm) exceeded the F_{ad} of the same polymer to a glass disc ($F_{ad} \sim 1{,}500$ mN for these asymmetric surfaces), and resulted in polymer damage during detachment (Fig. 3f). In contrast, a $t_c \sim 600$ s was required for the blocked catecholic polymer to exhibit the same level of damage on detachment.

In the case of the semi-rigid polymers (Fig. 3d), owing to the increase in polymer stiffness, F_{ad} of both the exposed and blocked catecholic polymers exhibited a low F_{ad} of ~50–70 mN up to a 'critical' t_c of 30 and 120 s, respectively. After the critical t_c, F_{ad} of the exposed catecholic polymer monotonically increased up to 820 mN at $t_c = 120$ s, whereas with blocked catechols F_{ad} increased to only 230 mN at $t_c = 3{,}600$ s. Also, the contact surface of the blocked catecholic polymer remained undamaged during detachment up to a $t_c = 3{,}600$ s (Fig. 3f).

For the rigid polymers (Fig. 3e), the effects of the low molecular mobility were more pronounced. No increase in F_{ad} was observed for the blocked catecholic polymer up to $t_c = 3{,}600$ s, whereas exposed catecholic polymers had a critical $t_c \sim 50$ s, which was larger than in the semi-rigid polymer. Consequently, F_{ad} increased to only 180 mN at $t_c = 3{,}600$ s in the rigid polymers.

Previous studies have proposed that the self-healing adhesion of catechol-functionalized polymers and proteins relies on the bidentate hydrogen bonding of catechols as well as on hydrophobic contributions[13,20,28]. If the same is true for catecholic polyacrylates, then molecular and polymer mobility should be important contributing factors. From the time- dependent adhesion tests (Fig. 3), we can conclude the following. First, bulk and surface molecular rearrangements are required to enable hydrogen bonding. The existence of a critical t_c indicates that the rearrangement/reorientation of polymer chains and molecular groups is a requisite for extensive interfacial hydrogen bonding. That the critical t_c increases with decreasing bulk and molecular mobility further supports this conclusion. Second, hydrogen-bond formation accelerates other attractive interactions. For the blocked catecholic semi-rigid polymer, F_{ad} increased only slightly (~230 mN m^{-1} at $t_c = 3{,}600$ s), whereas the adhesion of exposed catecholic polymer (Fig. 3d) increased from 70 to 820 mN at $t_c = 120$ s, which is significantly greater than the hydrogen-bond contribution of $F_{ad} \sim 300$ mN ($F_{ad,exposed} - F_{ad,blocked}$) measured for soft polymers at $t_c = 120$ s. This suggests that below a certain bulk/molecular mobility, hydrogen bonding is required to mobilize the other attractive interactions (for example, van der Waals, hydrophobic, polymer interdigitation, interpenetration, and interdiffusion) for self-healing.

Periodate stoichiometrically oxidizes catechol to quinone[29], hence was used to perturb intermolecular hydrogen bonding between symmetric catecholic soft polymer films (Fig. 4). With a $t_c = 5$ s and $L = 250$ mN, the soft polymer films achieved a $F_{ad} = 700$ mN. This force decreased monotonically with increasing [periodate] (Fig. 4I,II), ranging from all catechols (at 0 mM periodate; Fig. 4I) to all quinones (at 100 mM periodate; Fig. 4II). The latter resembled that of blocked catecholic polymers (Fig. 4a-III,b-III), suggesting no catecholic hydrogen-bond

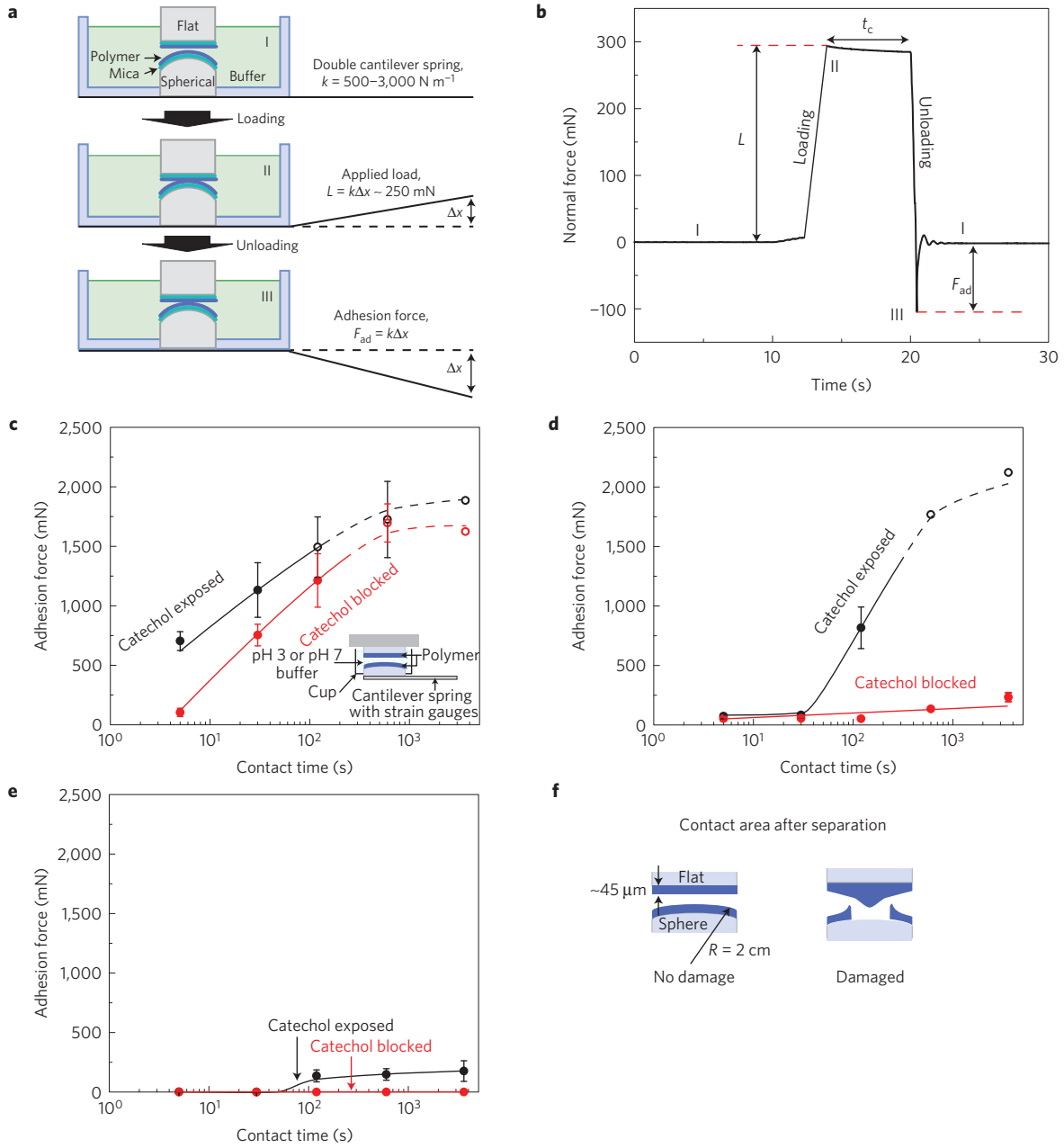

Figure 3 | Cohesive interactions between polymer films functionalized with exposed and blocked catechols as measured by the surface forces apparatus. a, Schematic of the symmetric surface geometry. **b**, An example of the measured normal-force signal when the surfaces are not in contact (I), and during loading (II) and unloading (III). **c**–**e**, Plots showing the force adhesion F_{ad} versus contact time t_c under an applied preload of $L \sim 250$ mN, between two soft/mobile (**c**), semi-rigid (**d**), and rigid polymeric surfaces (**e**). In **c**,**d**, the dashed lines and open circles indicate that polymer in the contact region becomes damaged on separation as shown in **f**. **f**, Schematics of undamaged and damaged surfaces.

contribution to adhesion. The importance of hydrogen bonding is further underscored by the adhesion tests using asymmetric film chemistry in which an all-catechol surface was brought into contact with an all-quinone surface (Fig. 4a-IV,b-IV). As this allows every catechol donor to hydrogen-bond to a quinone acceptor, this configuration gave forces comparable to or higher than those of symmetric catechol–catechol surfaces, where the catechols are both acceptors and donors.

The adhesion force from pure hydrogen bonding ($F_{ad,catechol/catechol} - F_{ad,quinone/quinone}$) was calculated to be 600 mN at $t_c = 5$ s. The catecholic bidentate hydrogen bond[30] has previously been reported to be around 67 ± 11 pN, which gives a catechol surface density of $\Gamma = 4.6 \times 10^{16}\ m^{-2}$ and a contact diameter of 0.5 mm in a contact about to detach. Assuming a flat surface with catechols distributed in a square lattice, the spacing between exposed catechols would be $\delta = (1/\Gamma)^{1/2} \approx 4.7 \pm 0.4$ nm. The high density of catechols at the interface is further compelling evidence for hydrogen-bond-initiated self-healing. However, we must emphasize that this prediction is valid only when intermolecular bidentate hydrogen bonding occurs, and some degree of multivalent hydrogen bonding is highly likely[24] (Fig. 1b).

Complete underwater self-healing in catechol-functionalized polyacrylates is initiated by intermolecular hydrogen bonding between interfacial catechol moieties, and subsequently consolidated by the recruitment of deeper physical interactions. This mechanism may explain the unusually strong and reversible adhesion measured between two dopa-containing mfp-5 films under reducing conditions[29]. More critically, it shows how simply

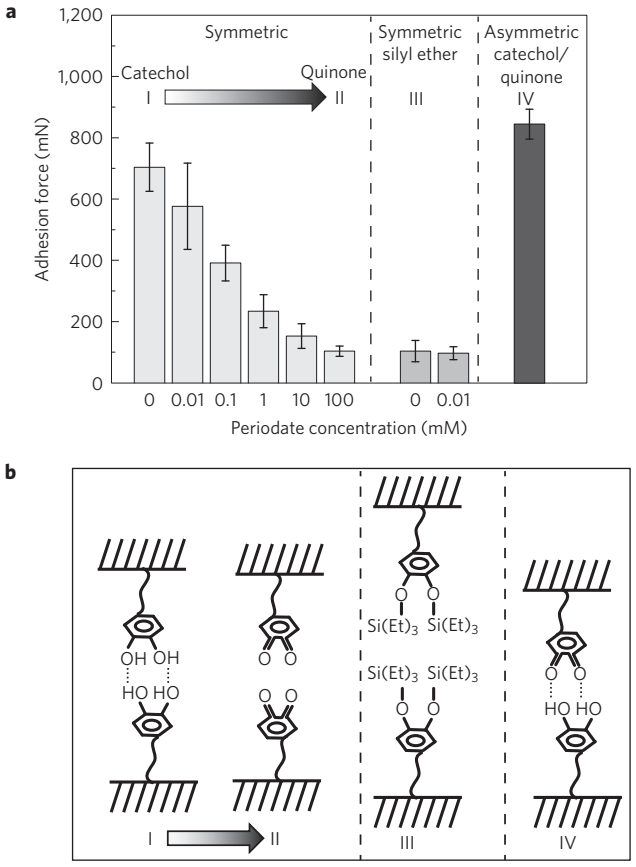

Figure 4 | Adhesion force between various polymeric surfaces with a contact time of 5 s and 250 mN of applied load. a, Catechol surfaces are partially (I) or fully (II) oxidized to quinone surfaces by adding different concentrations (0.01–100 mM) of periodate. Error bars indicate standard deviation, $n=5$. **b**, Proposed interfacial chemistry for I, II, III and IV.

re-engineering the surface of polyacrylate-based biomaterials can result in superior bulk self-mending properties. The need for improved self-mending in polyacrylates, for example, PMMA, is widely recognized[5]. Although the self-mending described here is limited to compliant materials at present, it holds considerable promise for the design of more durable implants in the future[6].

Methods

To prepare the underwater self-healing polymers, silane-protected eugenol acrylates (1 in Supplementary Fig. 1) and silane-protected methacrylates (2 in Supplementary Fig. 1) were synthesized on the basis of the previously reported silane protection of eugenol[14], epoxidation[31,32] and acrylation[33] of the alkene group, followed by ultraviolet radical polymerization (Supplementary Fig. 1). Ultraviolet radical polymerization was carried out with the Fusion ultraviolet system (Gaithersburg) that consisted of a 300 W inch^{-1} (2.54 cm) H lamp and LC6B benchtop conveyor belt. We prepared the polymers with a photoinitiator (Irgacure 819, bis-(2,4,6-trimethylbenzoyl)-phenylphosphineoxide), which was generously provided by BASF (Florham Park). Irgacure 819 at 1 wt% (0.01 g) was added to neat 1 or 2 (1 g) and the mixture was coated (thickness 25 μm) onto a substrate. Soft polymer sample was produced from 1 with 4 ultraviolet scans (ultraviolet radiation dose: 2,460–2,640 mJ cm^{-2}) whereas semi-rigid polymer required 8 scans (ultraviolet radiation dose: 4,920–5,280 mJ cm^{-2}). Rigid polymer sample was produced from 2 with 8 scans (ultraviolet radiation dose: 4,920–5,280 mJ cm^{-2}). The tensile strength (stress at break) was measured with a Bionix 200 tensile tester (MTS Systems). The polymer rods with 5 mm diameters were prepared by casting and kneading from the ultraviolet polymerized polymer films on a Teflon liner. The tensile strength distinguished the semi-rigid polymer with acrylate backbone (left in Supplementary Fig. 2) and the rigid polymer with methacrylate backbone (right in Supplementary Fig. 2). We bisected each polymer rod with a clean razor blade, and then soaked the pieces in buffers of different pH (pH 3, 7 and 10); the silyl-protecting groups of the catechols at the polymer surface were conveniently removed at low pH (pH 3 buffer) as previously reported[14] to expose superficial catechol moieties. It is unlikely that the pH 3 buffer removes all silyl groups at the interface; thus, quantification and optimization of silyl deprotection will require further future work. Subsequently, the tensile strength of each sample was measured to study the self-healing effect of surface catechol functionalities using an MTS tensile tester. NEXAFS were performed at the NIST/Dow soft X-ray materials characterization facility, beamline U7A at the National Synchrotron Light Source (NSLS) of Brookhaven National Laboratory. Carbon K-edge partial electron yield data were collected at a grid bias of −150 V. Contact angle measurements were performed using a custom-built contact angle goniometer. A sealed contact angle chamber was built of glass, and Teflon. A syringe needle was inserted through a hole at the top Teflon cap of the chamber and delivery was controlled from the outside by a motorized syringe device (KDS LEGATO270, Kd Scientific). A video camera was used to record the image of the drop. The air inside the chamber was saturated with water vapour for 30 min before experiments, maintaining the humidity at ~85%. The water droplet was infused for 2 min with the constant volumetric flow rate of 5 μl min^{-1} and was in rest for 60 min (Supplementary Fig. 8). The contact angle decreased with time (from 138° to 119°) and a three-phase contact line consequently crept out (horizontal arrows in Supplementary Fig. 8D). Contact line creep is an indicator of molecular turnover of polymers at the surface, for example, emersion of less hydrophobic polymers. The initial hydrophobicity returned when the surface was dried, suggesting a reversible rearrangement of the polymeric surfaces. In the SFA experiments, two glass discs (one spherical with $R=2$ cm, and one flat) were thoroughly cleaned with chloroform and ethanol. The spherical disc was firstly mounted into a custom-made 'cup' (Fig. 3a) before polymer deposition. The monomers (silane-protected eugenol acrylates or silane-protected methacrylates) were spread onto the glass discs and ultraviolet cured for predetermined times to achieve soft, semi-rigid or rigid polymeric surfaces (see ultraviolet polymerization section for details). For the contact time dependence experiment (Fig. 3), no additional modification was performed before mounting the surfaces into the SFA. For the experiment to check the effect of catechol oxidation (Fig. 4), catechol moieties at the surface were unblocked by soaking in pH 3 buffer for 30 min. Oxidation of catechols to orthoquinones was obtained by exposure to 0.01 mM–100 mM of periodate solution in pH 3 buffer for 10 min. The surfaces prepared as above were mounted in an SFA 2000 (ref. 34) attached with semiconductive strain gauges at double cantilever springs for load measurement[35]. Both surfaces were kept immersed in treatment buffer (pH 3 sodium acetate or pH 7 phosphate) using a miniaturized 'cup', which contains buffer reservoir (Fig. 3a). Loading and unloading were performed using a coarse micrometer which gives a maximum displacement of 0.5 cm at the velocity of ~2 mm s^{-1}. Depending on the stiffness of the double cantilever spring (up to ~3,000 N m^{-1}), this system can measure adhesion forces up to ~15 N. Applied load is determined by a change of the normal force signal to the positive direction and adhesion (pull out) force was measured by the negative normal force signal at which it jumped to zero normal force (Fig. 3b). For the first set of experiments (Fig. 3), after loading, the system was equilibrated for an adjustable contact time t_c (5–3,600 s) before unloading, to investigate the relation between the polymer rigidity, contact time and adhesion force. After unloading, the lower surface was dismounted from the SFA to check for damage. For the second set of experiments (Fig. 4), a fixed $t_c=5$ s was applied, and different surfaces were investigated to study the effects of hydrogen bonding on adhesion force. Applied loads L were set to 250 mN for all cases. Supplementary Figs 1–10 and associated Supplementary Refs (1–7) are available in the Supplementary Information.

Received 23 January 2014; accepted 17 June 2014; published online 27 July 2014

References

1. White, S. R. *et al.* Autonomic healing of polymer composites. *Nature* **409,** 794–797 (2001).
2. Ghosh, B. & Urban, M. W. Self-repairing oxetane-substituted chitosan polyurethane networks. *Science* **323,** 1458–1460 (2009).
3. Chen, X. X. *et al.* A thermally re-mendable cross-linked polymeric material. *Science* **295,** 1698–1702 (2002).
4. Cordier, P., Tournilhac, F., Soulie-Ziakovic, C. & Leibler, L. Self-healing and thermoreversible rubber from supramolecular assembly. *Nature* **451,** 977–980 (2008).
5. Dailey, M. M. *et al.* A self-healing biomaterial based on free-radical polymerization. *J. Biomed. Mater. Res.* http://dx.doi.org/10.1002/jbm.a.34975 (2013).
6. Boger, A., Heini, P., Windolf, M. & Schneider, E. Adjacent vertebral failure after vertebroplasty: A biomechanical study of low-modulus PMMA cement. *Eur. Spine J.* **16,** 2118–2125 (2007).
7. Holten-Andersen, N. *et al.* pH-induced metal–ligand cross-links inspired by mussel yield self-healing polymer networks with near-covalent elastic moduli. *Proc. Natl Acad. Sci. USA* **108,** 2651–2655 (2011).

8. Krogsgaard, M., Behrens, M. A., Pedersen, J. S. & Birkedal, H. Self-healing mussel-inspired multi-pH-responsive hydrogels. *Biomacromolecules* **14,** 297–301 (2013).
9. Shafiq, Z. *et al.* Bioinspired underwater bonding and debonding on demand. *Angew. Chem. Int. Ed.* **51,** 4332–4335 (2012).
10. Zeng, H., Hwang, D. S., Israelachvili, J. N. & Waite, J. H. Strong reversible Fe^{3+}-mediated bridging between dopa-containing protein films in water. *Proc. Natl Acad. Sci. USA* **107,** 12850–12853 (2010).
11. Holten-Andersen, N., Fantner, G. E., Hohlbauch, S., Waite, J. H. & Zok, F. W. Protective coatings on extensible biofibres. *Nature Mater.* **6,** 669–672 (2007).
12. Carrington, E. & Gosline, J. M. Mechanical design of mussel byssus: Load cycle and strain rate dependence. *Am. Malacol. Bull.* **18,** 135–142 (2004).
13. Yu, J. *et al.* Mussel protein adhesion depends on interprotein thiol-mediated redox modulation. *Nature Chem. Biol.* **7,** 588–590 (2011).
14. Heo, J. *et al.* Improved performance of protected catecholic polysiloxanes for bioinspired wet adhesion to surface oxides. *J. Am. Chem. Soc.* **134,** 20139–20145 (2012).
15. Menyo, M. S., Hawker, C. J. & Waite, J. H. Versatile tuning of supramolecular hydrogels through metal complexation of oxidation-resistant catechol-inspired ligands. *Soft Matter.* **9,** 10314–10323 (2013).
16. Sedó, J., Saiz-Poseu, J., Busqué, F. & Ruiz-Molina, D. Catechol-based biomimetic functional materials. *Adv. Mater.* **25,** 653–701 (2013).
17. Belman, N., Jin, K. J., Golan, Y., Israelachvili, J. N. & Pesika, N. S. Origin of the contact angle hysteresis of water on chemisorbed and physisorbed self-assembled monolayers. *Langmuir* **28,** 14609–14617 (2012).
18. Eslami, M., Zare, H. R. & Namazian, M. Thermodynamic parameters of electrochemical oxidation of L-DOPA: Experimental and theoretical studies. *J. Phys. Chem. B* **116,** 12552–12557 (2012).
19. Lee, B. P., Messersmith, P. B., Israelachvili, J. N. & Waite, J. H. in *Annual Review of Materials Research* Vol. 41 (eds Clarke, D. R. & Fratzl, P.) 99–132 (Annual Reviews: Palo Alto, 2011).
20. Yu, J. *et al.* Adaptive hydrophobic and hydrophilic interactions of mussel foot proteins with organic thin films. *Proc. Natl Acad. Sci. USA* **110,** 15680–15685 (2013).
21. Zhang, J. *et al.* Real-space identification of intermolecular bonding with atomic force microscopy. *Science* **342,** 611–614 (2013).
22. Aviram, A., Seiden, P. E. & Ratner, M. A. in *Molecular Electronic Devices* (ed. Carter, F. L.) 5–17 (Marcel Dekker, 1983).
23. Tylli, H. & Konschin, H. A Raman spectroscopic study of the OH and OD torsion in 1,2-dihydroxybenzene. *J. Mol. Struct.* **57,** 13–19 (1979).
24. Navarrete, J. T. L. & Ramírez, F. J. A study by Raman spectroscopy and the semiempirical AM1 method on several 1,2-dihydroxybenzene solutions. *Spectrochim. Acta A* **49,** 1759–1767 (1993).
25. Hemraj-Benny, T. *et al.* Near-edge X-ray absorption fine structure spectroscopy as a tool for investigating nanomaterials. *Small* **2,** 26–35 (2006).
26. Park, J. *et al.* Structural characterization of conjugated polyelectrolyte electron transport layers by NEXAFS spectroscopy. *Adv. Mater.* **20,** 2491–2496 (2008).
27. Lee, D. W., Lim, C., Israelachvili, J. N. & Hwang, D. S. Strong adhesion and cohesion of chitosan in aqueous solutions. *Langmuir* **29,** 14222–14229 (2013).
28. Anderson, T. H. *et al.* The contribution of DOPA to substrate–peptide adhesion and internal cohesion of mussel-inspired synthetic peptide films. *Adv. Funct. Mater.* **20,** 4196–4205 (2010).
29. Danner, E. W., Kan, Y. J., Hammer, M. U., Israelachvili, J. N. & Waite, J. H. Adhesion of mussel foot protein Mefp-5 to mica: An underwater superglue. *Biochemistry* **51,** 6511–6518 (2012).
30. Wang, J. *et al.* Influence of binding-site density in wet bioadhesion. *Adv. Mater.* **20,** 3872–3876 (2008).
31. Ahn, B. K., Kraft, S. & Sun, X. S. Chemical pathways of epoxidized and hydroxylated fatty acid methyl esters and triglycerides with phosphoric acid. *J. Mater. Chem.* **21,** 9498–9505 (2011).
32. Ahn, B. K., Kraft, S., Wang, D. & Sun, X. S. Thermally stable, transparent, pressure-sensitive adhesives from epoxidized and dihydroxyl soybean oil. *Biomacromolecules* **12,** 1839–1843 (2011).
33. Bunker, S. P. & Wool, R. P. Synthesis and characterization of monomers and polymers for adhesives from methyl oleate. *J. Polym. Sci. Polym. Chem.* **40,** 451–458 (2002).
34. Israelachvili, J. *et al.* Recent advances in the surface forces apparatus (SFA) technique. *Rep. Prog. Phys.* **73,** 036601 (2010).
35. Lee, D. W., Banquy, X. & Israelachvili, J. N. Stick–slip friction and wear of articular joints. *Proc. Natl Acad. Sci. USA* **110,** E567–E574 (2013).

Acknowledgements

The authors gratefully acknowledge financial support from the Office of Naval Research N000141310867, the United Soybean Board, the Institute for Collaborative Biotechnologies through grant W911NF-09-0001 from the US Army Research Office (the content of the information does not necessarily reflect the position or the policy of the Government, and no official endorsement should be inferred), the National Science Foundation MRSEC DMR-1121053, and the US Department of Energy, Office of Basic Energy Sciences, Division of Materials Sciences under Award DE-FG02-87ER-45331 (J.N.I. for the instrument modification of the Surface Forces Apparatus for the adhesion measurements and D.W.L. for the adhesion measurements). The authors also acknowledge assistance from T. Mates for XPS, Y. Li for XRR, and L. Perez for NEXAFS and GIWAXS.

Author contributions

B.K.A. and D.W.L designed the research, performed the experiments, and wrote the paper. J.N.I. advised the experimental design of the modified SFA and experimental measurements, and the interpretation of results. J.H.W. supervised the overall experimental design and writing.

Additional information

Supplementary information is available in the online version of the paper. Reprints and permissions information is available online at www.nature.com/reprints. Correspondence and requests for materials should be addressed to J.N.I. or J.H.W.

Competing financial interests

The authors declare no competing financial interests.